Catalyst and Chirality Dependent Growth of Carbon Nanotubes Determined Through Nano-Test Tube Chemistry

By *Hidetsugu Shiozawa,* Christian Kramberger, Rudolf Pfeiffer, Hans Kuzmany, Thomas Pichler, Zheng Liu, Kazu Suenaga, Hiromichi Kataura,* and *S. Ravi P. Silva**

Single-walled carbon nanotubes (SWCNTs) have attracted much interest for their unique nanostructural and electronic properties, which have a wide range of potential applications. The key barrier that prevents SWCNTs fulfilling their potential in electronic applications is the understanding of the growth mechanism and, as a consequence, the inability to control the tube size, chirality, and hierarchy in the structure on a bulk scale. The synthesis of SWCNTs in general requires metal nanocompounds to catalyze the growth. Notably successful catalysts include Fe, Ni, and Co. Noble metals (Au, Ag, Pt, and Pd) have recently been reported to catalyze the growth of carbon nanotubes as well.[1,2] While recent improvements in yield, purity, and selectivity were obtained by using a variety of bulk synthesis techniques, individual chemical processes have rarely been observed.

Nano-test tube chemistry uses the hollow space inside SWCNTs as a controlled local environment to perform syntheses. The hollow space inside SWCNTs can be utilized for the encapsulation of atoms and molecules in a highly controlled manner. A large variation of fullerene materials and organic molecules have thus far been encapsulated inside carbon nanotubes.[3–12] Such filled nanotubes allow chemical reactions to be confined at the nanometer-scale such that novel chemistry processes can occur and the individual chemical events can be observed at the molecular level.

Preliminary research on nano-test tube chemistry includes the transformation of SWCNTs encapsulating molecules into double-walled carbon nanotubes (DWCNTs).[11–15] It has been reported that the encapsulated reactions can also lead to functionalization of the original carbon nanotubes.[16,17] These papers highlight the potential merits of encapsulation and nano-test tube chemistry for the study of carbon nanotube growth as well as for their functionalization.

In this paper, using the highly confined and controlled volumetric space within a nano-test tube we study the growth properties of SWCNTs. Two types of metals used frequently in the catalytic growth of carbon nanotubes, Pt and Fe, are chosen as model catalysts to grow inner tubes. To this end, two organometallic compounds, Pt(II) acetylacetonate (PtAc), $Pt(C_5H_7O_2)_2$, and ferrocene, $Fe(C_5H_5)_2$, are encapsulated inside SWCNTs as precursors (see Supporting Information). The growth process of the inner tube is traced by high-resolution transmission electron microscopy (HRTEM) which allows monitoring of an individual tube as it grows out of a Pt nanocrystal. Raman spectroscopy reveals that the inner tubes grow differently based on the catalytic reaction temperature. At the low temperature limits, DWCNTs of optimal interwall distances are found to grow. In such DWCNTs the intertube interaction is too small to be resolved by Raman scattering. It means that the inner tubes are well distanced from the outer tubes and the growth process is solely determined by the nature of the catalytic metal. It is found that thinner tubes grow at lower temperatures, which points to a lower activation energy for the thinner SWCNT growth. Furthermore, the catalytic tube growth with Fe occurs at lower temperatures than with Pt. As an example, the (6,4) tube growth is found to be activated at 700 °C with Pt catalyst, while it grows well at 500 °C with Fe catalysts. The assigned activation temperature for catalytic tube growth is fundamental when the diameter of the carbon nanotubes is a requirement that needs to be controlled on a bulk scale and, therefore, the growth mechanism needs to be well understood. Only studies that utlize nano-test tube chemistry allow the growth parameters to be determined for a given chirality with high accuracy. Hence, the outcome of this study opens a pathway for the control of the growth of carbon nanotubes as building blocks for future nanotechnology.

Figure 1a shows a room-temperature HRTEM micrograph of the PtAc-filled SWCNTs (PtAc@NT) annealed at 700 °C. It is observed at the atomic scale that a thin tube is connected with its open end to a nanocrystal inside a SWCNT. The interplanar distances of the nanocrystal agree with those of a Pt crystal within the limits of experimental error, and are significantly different from the Pt carbide crystal structures reported thus far. Analyses from electron energy-loss spectroscopy (EELS) also demonstrate the encapsulation of Pt particles inside SWCNTs (see Supporting Information). Further HRTEM observations with in-situ annealing up to 760 °C confirm that the inner tube wall remains terminated at a Pt crystal even at the growth temperature of 760 °C, as shown in Figure 1b. The growth stops

[*] Dr. H. Shiozawa, Prof. S. R. P. Silva
Advanced Technology Institute
University of Surrey
Guildford, GU2 7XH (UK)
E-mail: h.shiozawa@surrey.ac.uk; s.silva@surrey.ac.uk
Dr. C. Kramberger, Dr. R. Pfeiffer, Prof. H. Kuzmany, Prof. T. Pichler
Faculty of Physics
University of Vienna
Strudlhofgasse 4, 1090, Vienna (Austria)
Dr. Z. Liu, Dr. K. Suenaga
Research Center for Advanced Carbon Materials
AIST, Tsukuba, 305-8565 (Japan)
Dr. H. Kataura
Nanotechnology Research Institute
AIST, Tsukuba 305-8562 and JST, CREST (Japan)

DOI: 10.1002/adma.201001211

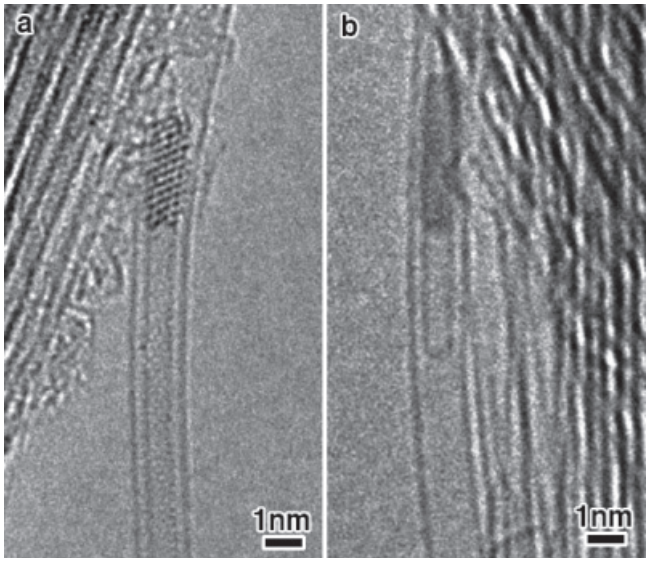

Figure 1. TEM micrographs for PtAc@NT ex-situ annealed at 700 °C for 2 h (a) and in-situ annealed at temperatures up to 760 °C (b).

when the entire carbon source is exhausted with the tube end remaining on the Pt surface. This is unlikely to be seen in SWCNT samples obtained from conventional bulk-scale synthesis where catalytic particles are usually observed to be encapsulated by graphitic carbons. On the bulk scale synthesis the growth of SWCNT stops when the catalytic nanoparticle becomes inactive because of graphitic layers and/or closed tube ends formed around the surface. In contrast, inside a SWCNT acting as a perfect nano-clean room, the growth condition is homogeneous and constant. Any unfavourable fluctuations in growth conditions that usually cause graphitization of the nanoparticle surface are absent inside SWCNTs. As a consequence, the inner tube can continue to grow until all the carbon atoms are used up. The reaction stops at this point, but the encapsulated system remains at this point at which the HRTEM snapshot is obtained.

FT Raman spectra of the empty SWCNT (NT) and PtAc@NT before and after annealing at different temperatures in the range from 300 to 1200 °C are compared in **Figure 2a**. The radial breathing mode (RBM) lines for the original SWCNT appear as two peaks located at frequencies ranging from 150 to 200 cm^{-1}. A double peak located around 310–370 cm^{-1} can be assigned to the second order for the original tube RBM lines. By inspecting the spectra of the samples annealed at different temperatures, the inner tubes are found to grow at temperatures higher than 600 °C. The growth properties depend strongly on the temperature. After annealing at a high temperature of 1200 °C many sharp peaks appear at frequencies ranging from 300 to 340 cm^{-1}. The line distribution is very similar to that observed previously for DWCNTs transformed from ferrocene-filled SWCNTs and is attributed to the RBM lines for the inner tubes grown from the encapsulated PtAc molecules.[11] Due to the van der Waals interaction between the inner tube and outer tube, an inner tube in a thinner outer tube gives rise to the RBM line at a higher frequency. From a comparison to the extended tight-binding model, the peaks

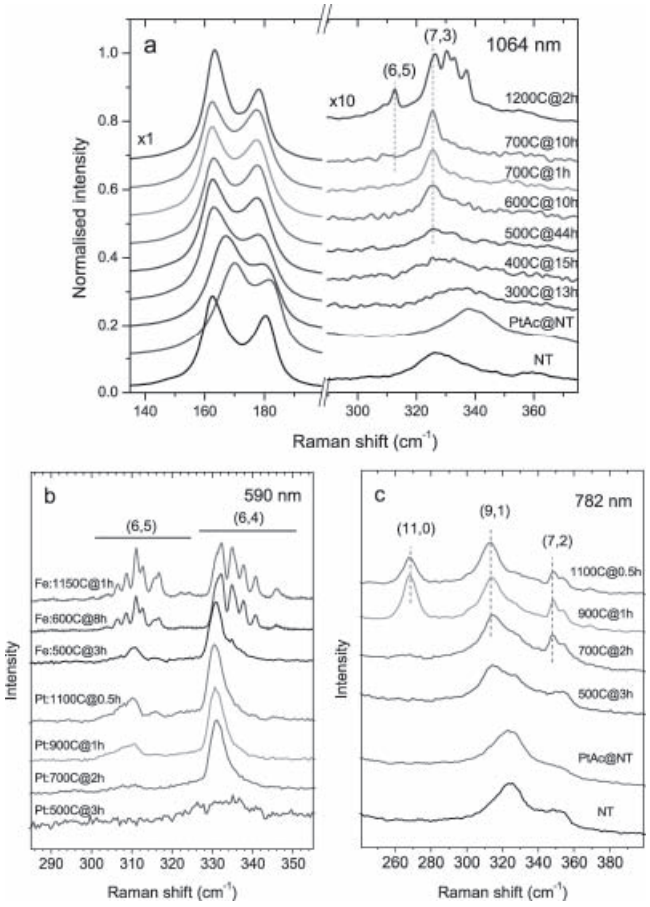

Figure 2. a) FT Raman spectra obtained at a wavelength of 1064 nm for the empty SWCNT (NT) and PtAc@NT before and after being annealed at various temperatures and durations. b) Raman spectra obtained at 590 nm for the annealed PtAc@NT samples (lower set of spectra) and for the annealed ferrocene-filled SWCNTs (upper set of spectra). c) Raman spectra collected at 782 nm for the empty SWCNT (NT) and the pristine and annealed PtAc@NT samples.

located around 312 cm^{-1} and those at frequencies higher than 325 cm^{-1} can be assigned as the RBM lines for the (6,5) and (7,3) inner tubes in different outer tubes, respectively.[18,19] On the contrary, after annealing at 600 and 700 °C only one prominent peak appears at 325 cm^{-1}. This line is assigned as the RBM of the (7,3) tubes inside the outer tubes with diameters larger than 1.40 nm. The RBM lines for the (6,5) tubes are hardly observed in these samples. These results show that at low temperatures thinner inner tubes with larger intra-tube distances grow predominantly.

The lower set of spectra in Figure 2b are the Raman spectra obtained at 590 nm for the PtAc@NT annealed at 500 °C for 3 h, 700 °C for 2 h, 900 °C for 1 h, and 1100 °C for 30 min. For the samples annealed at temperatures higher than 700 °C two peaks are predominantly observed around 310 and 331 cm^{-1}. They are, as before,[11,19] assigned to the RBM lines of the (6,5) and (6,4) inner tubes. Importantly, again no higher frequency lines corresponding to the inner tubes inside thinner outer tubes are observed. This is consistent with the FT Raman data and indicates very weak van der Waals interactions between the inner

and outer tubes. This line shape is retained for the DWCNT samples transformed at temperatures up to 1100 °C. In other words, for those DWCNTs grown at temperatures between 700 and 1100 °C the inner tube diameter is optimally determined by the outer tube diameter. From a detailed comparison to the extended tight-binding model, we evaluate the corresponding outer tube diameters to be larger than 1.40 nm.[11,18,19] The size of the DWCNT observed in the HRTEM micrograph in Figure 1a matches very well with the (6,4) tube encapsulated inside a tube with a diameter of 1.5 nm. This result supports our conclusion that inner tubes are well distanced from outer tubes when they grow at low enough temperatures.

It is important to note that DWCNTs with non-interacting inner tube–outer tube pairs can only be grown by catalytic reactions. In the present case Pt acts as a catalyst for the inner tube growth. It has recently been reported that noble elements (Au, Ag, Pt, and Pd) can catalyze the growth of SWCNTs by chemical vapor deposition and arc discharge methods.[1] This is rather surprising taking into account that noble metals are relatively inert in comparison to Fe, Co, and Ni, which tend to have high binding energies with carbon required for the formation of a graphitic network. Yet the exact role of metal elements on the growth of SWCNTs remains elusive. Our result clearly shows that Pt acts as a catalyst and its activation temperature for the SWCNT growth can be as low as 600 °C. It has been suggested that the size of the metal particle determines the diameter of the SWCNTs to be grown. In the case of catalytic inner tube growth, the metal nanocrystals nucleate and grow the inner tube, as observed in the HRTEM micrographs in Figure 1. The size of the nanocrystal is defined by the confinement of the original tube, and the inner tube growth properties depend solely on the type of metal.

Based on this fact, it would be interesting to compare the encapsulated catalytic properties of Pt with those of a conventional catalyst such as Fe. Corresponding results are depicted in Figure 2b, where the RBM lines for the (6,4) and (6,5) inner tubes grown from an encapsulated ferrocene precursor (upper set of spectra) are compared with those from the PtAc precursor (lower set of spectra). A feature similar to the Pt case is observed for DWCNTs grown at the lowest growth temperature of 500 °C with Fe, which is lower by 200 °C in comparison to the temperature required for the same chirality of inner tubes to be grown from PtAc. As shown in Figure 2b, at 500 °C no inner tubes can grow from the Pt precursor. This is direct evidence that the activation temperature for SWCNT growth is higher with a Pt catalyst. For the DWCNTs grown with Fe at temperatures higher than 600 °C a variety of inner tube RBM lines that correspond to the (6,4) and (6,5) inner tubes inside thinner outer tubes are observed, as reported previously.[11] This is in good agreement with the case for the (7,3) inner tubes grown with a Pt catalyst at higher temperatures, as observed in Figure 2a, and confirms for both Pt and Fe catalysts that only at low temperatures the inner tube becomes well distanced from the outer tube.

Furthermore, with a Pt catalyst, almost only the thinner (6,4) tube can grow at 700 °C while both the (6,4) and (6,5) tubes can grow at higher temperatures, as observed in Figure 2b. This means that thinner inner tubes preferentially grow at a low temperature, again in accordance with the FT Raman results in Figure 2a where the (7,3) tube grows while the (6,5) tube does not at 700 °C.

This point is further investigated for other chirality tubes. Figure 2c shows the Raman spectra collected at 782 nm for the pristine and annealed PtAc@NT samples. At this wavelength the (11,0), (9,1), and (7,2) inner tubes are in resonance and their RBM lines appear at 268, 313, and 348.5 cm^{-1}, respectively, after annealing. At a low temperature of 700 °C only the thinner two tubes, (9,1) and (7,2), are grown. Similarly, from Raman spectroscopy using a wavelength of 514 nm, the (8,2) tube is found to grow only at temperatures higher than 700 °C with Pt catalyst. Among those inner tubes grown at 700 °C with Pt, the (9,1) tube has the largest diameter of 0.754 nm. It is, therefore, the largest diameter of the inner tube grown at 700 °C. The presence of a maximum threshold for the inner tube diameter at a fixed reaction temperature is of great importance. It tells us about the nature of the SWCNT growth in a sense that the activation energy is lower for thinner diameter tubes. This is in line with previously reported observations on the bulk scale synthesis of SWCNTs where thinner tubes tend to grow at lower furnace temperatures.[20–24] Our nano-test tube chemistry combined with resonance Raman spectroscopy allows the activation temperatures to be precisely assigned for pure metal catalysts and for tubes of specific chiralities. This finding is visualized on the map of chiral vectors in **Figure 3**. The (9,1) tube with a diameter of 0.754 nm is found to grow at temperatures higher than 700 °C with Pt catalyst. In other words, only the tubes thinner than the (9,1) tube within the blue shaded arc can grow under these conditions. At higher temperatures, the larger diameter tubes in the red shaded area can also grow. The activation temperature for the (9,1) tube growth with Pt catalyst, $T_{Pt}^{(9,1)}$= 700 °C, can be denoted by the arced arrow whose length is proportional to the tube diameter assumed to follow a linear relation to each other and is scaled depending on the type of catalyst, i.e., $T_{Pt}^{(9,1)} > T_{Fe}^{(9,1)}$.

According to the vapor–liquid–solid model, the activation energy of the tube growth is determined by the thermodynamics of the catalyst particle, the solubility of carbon, the kinetics of carbon diffusion, and their interactions with substrates. In our test tube experiments the outer tube confines the precursor elements and growth process, and the growth temperature is determined at the thermodynamic equilibrium. In this case, the carbon diffusion kinetics that influence the growth rate is insignificant to the growth properties for different tube diameters. Hence, the catalytic activity of the metal–carbon system is predominantly correlated with the eutectic point that varies for different particle sizes and metal elements.[25] The reduction of the melting point of a spherical metal nanoparticle is known to be proportional to the inverse of the particle radius, as described by the model based on the Gibbs–Thomson equation:

$$T_m(\infty) - T_m(r) = \frac{2T_m(\infty)\sigma_{SL}}{\Delta H_f(\infty)\rho_s}\frac{1}{r} \quad (1)$$

where $T_m(\infty)$, σ_{SL}, $\Delta H_f(\infty)$, and ρ_s are the bulk melting temperature, the solid–liquid interfacial energy, the bulk latent heat of fusion, and the number of the solid phase, respectively. $T_m(r)$ represents the melting point of a freestanding spherical particle

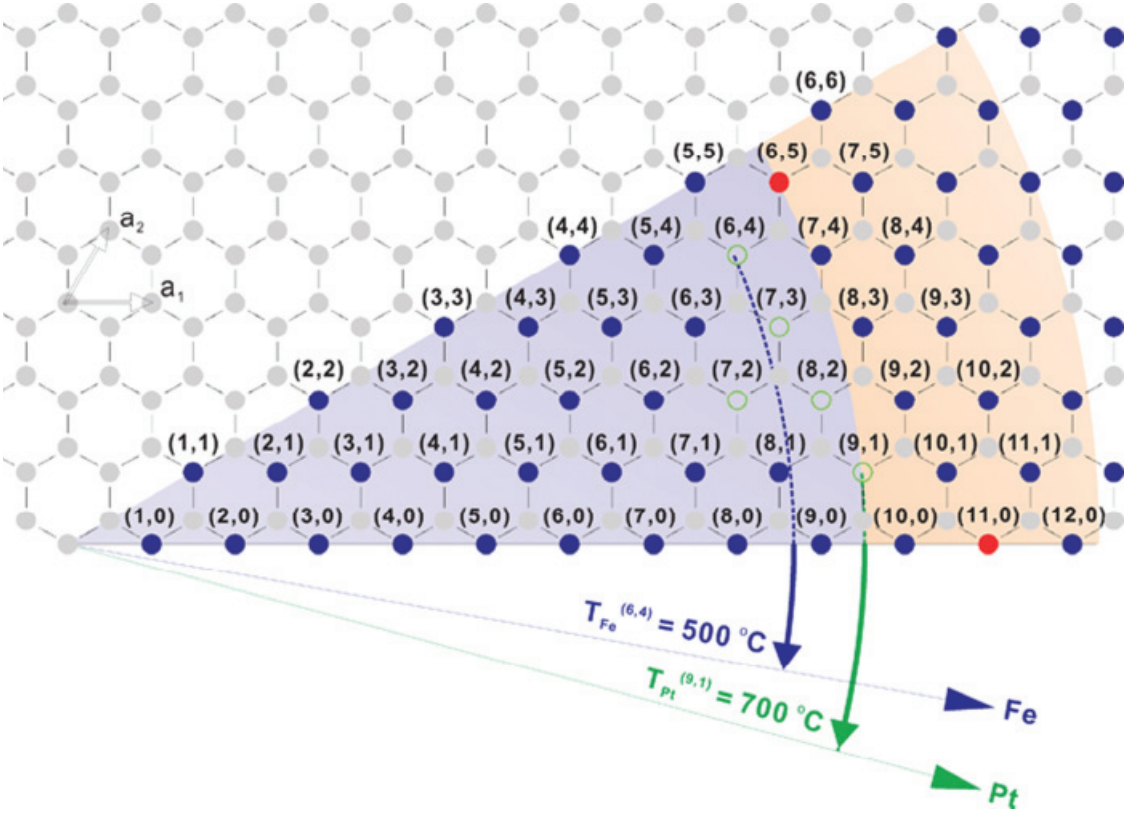

Figure 3. On the map of chiral vectors the green open circles are the tubes (7,2), (6,4), (7,3), (8,2), and (9,1) that can grow at 700 °C with Pt, while the red solid circles are the tubes (6,5) and (11,0) that need temperatures higher than 700 °C to grow. At 700 °C only the tubes in the blue shaded area can grow with Pt catalyst. At higher temperatures the thicker tubes in the red shaded area can also grow. The activation temperature for the (9,1) tube growth with Pt catalyst, $T_{Pt}^{(9,1)}$ = 700 °C, is represented by the green solid arced arrow. In a similar way, the activation temperature for the (6,4) tube growth with Fe, $T_{Fe}^{(6,4)}$ = 500 °C, can be represented by the blue solid arced arrow.

with radius r. The linear slope of the temperature reduction against the inverse radius gives the Gibbs–Thomson coefficient that is reported to be about 2×10^{-7} K m for pure iron particles.[26,27] Using the Fe-C liquefaction point of $T_m^{FeC}(\infty)$ = 1403 K, reduced from $T_m^{Fe}(\infty)$ = 1811 K for a pure Fe, we obtain a melting point of about 823 K for a freestanding iron carbide nanoparticle with a radius of 0.345 nm. Provided that the inner tube has a similar radius to the catalyst particle, this value is in line with the activation temperature of 773 K for the (6,4) tube of the same radius as the Fe catalyst. The further reduction by 50 K could be attributable to the predominant surface diffusion[28] that competes against the reduced solubility[29] and the interaction with the substrate.

Little is known about the melting point of Pt nanoparticles. From a linear fit of the previously reported data,[30–32] a Gibbs–Thomson coefficient of 8.4×10^{-7} K m can be obtained for a freestanding platinum nanoparticle. Substituting the melting point of the bulk Pt-C system, $T_m^{PtC}(\infty)$ = 2011 K, we obtain a melting point of 797 K for a Pt-C nanoparticle with a radius of 0.375 nm. It was reported that the Gibbs–Thomson coefficient increases with increasing melting point.[33] Extrapolating a linear fit of the previously reported melting point data for Cr, Fe, Mo, and W nanoparticles to the Pt case, we can obtain another value of 2.5×10^{-7} K m and the melting point of 1334 K for a Pt-C nanoparticle with a radius of 0.375 nm. Both melting points do not coincide with the present study, where the activation temperature of 973 K for the (9,1) tube with a radius of 0.375 nm is obtained for the Pt catalyst. These discrepancies are likely a result of the inaccurate Gibbs–Thomson coefficient values estimated from the limited number of data from the multiple references. To the best of our knowledge, no Gibbs–Thomson coefficient value for Pt has been reported so far. In other words, using the activation temperature of 973 K for the (9,1) tube, a real Gibbs–Thomson coefficient value for Pt is estimated to be 3.64×10^{-7} K m.

To conclude, it is crucial to lower the growth temperature in order for better compatibility of carbon nanotubes with electronics.[34,35] The inside of carbon nanotubes is free from contamination. Encapsulated molecules provide both catalysts and carbon sources in a highly controlled proportion. Hence, our nano-test tube chemistry offers a very efficient and controlled route to SWCNT synthesis. There is also the intriguing possibility for a follow-up study on material filling the SWCNT and seeding further growth once the caps of the outer layer have been removed. Further studies using various organometallic compounds as precursors will facilitate a comprehensive understanding of the mechanism for the catalytic growth of SWCNT.

Experimental Section

SWCNT material with a diameter range of 1.4 ± 0.1 nm was synthesized by laser ablation and purified by H_2O_2 treatment.[36] The tube material was pre-treated by annealing in air at 400 °C for 20 min to open the tube caps. The open-ended SWCNTs were then dipersed in acetone with PtAc and sonicated overnight for filling. Filling with ferrocene was performed by exposure of the SWCNT film to a vapor phase of ferrocene at 150 °C for several days in a sealed Pyrex glass ampule.[11] The filled SWCNT films of the same batch were transformed into DWCNTs by annealing in vacuum at different temperatures. Raman spectra of the empty, filled, and annealed samples were recorded at room temperature using a Bruker FT Raman spectrometer with a wavelength of 1064 nm and a Renishaw 2000 microRaman spectrometer with wavelengths of 782 and 514 nm, and at 80 K using a Dilor XY triple spectrometer at 590 nm. HRTEM was performed with a JEM-2010F microscope equipped with a Cs corrector at an accelerating voltage of 80 kV. Gatan ENFINA adjusted for a 60 kV incident electron beam was used for EELS chemical analyses on a JEOL-2100F equipped with an aberration corrector (the DELTA-corrector).

Supporting Information

Supporting Information is available online from Wiley InterScience or from the author.

Acknowledgements

H. S. acknowledges the Leverhulme Trust for support through an early career fellowship. S. R. P. S. thanks the EPSRC for financial support through a Portfolio Partnership award. R. P. acknowledges financial support from FWF project I83-N20 (ESF IMPRESS). L. Z. and K. S. acknowledge the support of the Japan Science and Technology Agency–Core Research for Evolutional Science and Technology. The authors thank R. Schönfelder, S. Leger, R. Hübel, H. Klose, C. Buxey, J. Underwood, D. Mansfield, C. Shaw, and M. Blissett for technical assistance.

Received: April 3, 2010
Published online: June 9, 2010

[1] D. Takagi, Y. Homma, H. Hibino, S. Suzuki, Y. Kobayashi, *Nano Lett.* **2006**, *6*, 2642.
[2] D. Yuan, L. Ding, H. Chu, Y. Feng, T. P. McNicholas, J. Liu, *Nano Lett.* **2008**, *8*, 2576.
[3] B. W. Smith, M. Monthioux, D. E. Luzzi, *Nature* **1998**, *396*, 323.
[4] J. Lee, H. Kim, S. J. Kahng, G. Kim, Y. W. Son, J. Ihm, H. Kato, Z. W. Wang, T. Okazaki, H. Shinohara, Y. Kuk, *Nature* **2002**, *415*, 1005.
[5] D. J. Hornbaker, S.-J. Kahng, S. Misra, B. W. Smith, A. T. Johnson, E. J. Mele, D. E. Luzzi, A. Yazdani, *Science* **2002**, *295*, 828.
[6] T. Takenobu, T. Takano, M. Shiraishi, Y. Murakami, M. Ata, H. Kataura, Y. Achiba, Y. Iwasa, *Nat. Mater.* **2003**, *2*, 683.
[7] L. J. Li, A. N. Khlobystov, J. G. Wiltshire, G. A. D. Briggs, R. J. Nicholas, *Nat. Mater.* **2005**, *4*, 481.
[8] K. Yanagi, Y. Miyata, H. Kataura, *Adv. Mater.* **2006**, *18*, 437.
[9] Z. Liu, K. Yanagi, K. Suenaga, H. Kataura, S. Iijima, *Nat. Nanotechnol.* **2007**, *2*, 422.
[10] T. Pichler, *Nat. Mater.* **2007**, *6*, 332.
[11] H. Shiozawa, T. Pichler, A. Grüneis, R. Pfeiffer, H. Kuzmany, Z. Liu, K. Suenaga, H. Kataura, *Adv. Mater.* **2008**, *20*, 1443.
[12] R. Kitaura, N. Imazu, K. Kobayashi, H. Shinohara, *Nano Lett.* **2008**, *8*, 693.
[13] S. Bandow, M. Takizawa, K. Hirahara, M. Yudasaka, S. Iijima, *Chem. Phys. Lett.* **2001**, *337*, 48.
[14] R. Pfeiffer, H. Kuzmany, Ch. Kramberger, Ch. Schaman, T. Pichler, H. Kataura, Y. Achiba, J. Kürti, V. Zólyomi, *Phys. Rev. Lett.* **2003**, *90*, 225 501.
[15] R. Pfeiffer, M. Holzweber, H. Peterlik, H. Kuzmany, Z. Liu, K. Suenaga, H. Kataura, *Nano Lett.* **2007**, *7*, 2428.
[16] H. Shiozawa, T. Pichler, C. Kramberger, A. Grüneis, M. Knupfer, B. Büchner, V. Zólyomi, J. Koltai, J. Kürti, D. Batchelor, H. Kataura, *Phys. Rev. B* **2008**, *77*, 153 402.
[17] H. Shiozawa, T. Pichler, C. Kramberger, M. Rümmeli, D. Batchelor, Z. Liu, K. Suenaga, H. Kataura, S. R. P. Silva, *Phys. Rev. Lett.* **2009**, *102*, 046 804.
[18] V. N. Popov, *New J. Phys.* **2004**, *6*, 17.
[19] R. Pfeiffer, F. Simon, H. Kuzmany, V. N. Popov, *Phys. Rev. B* **2005**, *72*, 161 404.
[20] H. Kataura, Y. Kumazawa, Y. Maniwa, Y. Ohtsuka, R. Sen, S. Suzuki, Y. Achiba, *Carbon* **2000**, *38*, 1691.
[21] Y. Miyauchi, S. Chiashi, Y. Murakami, Y. Hayashida, S. Maruyama, *Chem. Phys. Lett.* **2004**, *387*, 198.
[22] Y. Li, S. Peng, D. Mann, J. Cao, R. Tu, K. J. Cho, H. Dai, *J. Phys. Chem. B* **2005**, *109*, 6968.
[23] A. Barreiro, S. Hampel, M. H. Rümmeli, C. Kramberger, A. Grüneis, K. Biedermann, A. Leonhardt, T. Gemming, B. Büchner, A. Bachtold, T. Pichler, *J. Phys. Chem. B* **2006**, *110*, 20 973.
[24] M. H. Rümmeli, C. Kramberger, M. Löffler, O. Jost, M. Bystrzejewski, A. Grüneis, T. Gemming, W. Pompe, B. Büchner, T. Pichler, *J. Phys. Chem. B* **2007**, *111*, 8234.
[25] M. Takagi, *J. Phys. Soc. Jpn.* **1954**, *9*, 359.
[26] D. Turnbull, *J. Appl. Phys.* **1950**, *21*, 1022.
[27] Y. Shibuta, Y. Watanabe, T. Suzuki, *Chem. Phys. Lett.* **2009**, *475*, 264.
[28] V. Stolojan, Y. Tison, G. Y. Chen, R. Silva, *Nano Lett.* **2006**, *6*, 1837.
[29] A. R. Harutyunyan, N. Awasthi, A. Jiang, W. Setyawan, E. Mora, T. Tokune, K. Bolton, S. Curtarolo, *Phys. Rev. Lett.* **2008**, *100*, 195 502.
[30] B. H. Morrow, A. Striolo, *Nanotechnology* **2008**, *19*, 195 711.
[31] B. H. Morrow, A. Striolo, *J. Phys. Chem. C* **2007**, *111*, 17 905.
[32] Y. Wen, H. Fang, Z. Zhu, S. Sun, *Chem. Phys. Lett.* **2009**, *471*, 295.
[33] Y. Shibuta, T. Suzuki, *J. Chem. Phys.* **2008**, *129*, 144 102.
[34] M. Cantoro, S. Hofmann, S. Pisana, V. Scardaci, A. Parvez, C. Ducati, A. C. Ferrari, A. M. Blackburn, K-Y. Wang, J. Robertson, *Nano Lett.* **2006**, *6*, 1107.
[35] E. Mora, J. M. Pigos, F. Ding, B. I. Yakobson, A. R. Harutyunyan, *J. Am. Chem. Soc.* **2008**, *130*, 11 840.
[36] H. Kataura, Y. Maniwa, M. Abe, A. Fujiwara, T. Kodama, K. Kikuchi, H. Imahori, Y. Misaki, S. Suzuki, Y. Achiba, *Appl. Phys. A* **2002**, *74*, 349.